Chemical Engineering Science 152 (2016) 163–171

Contents lists available at ScienceDirect

Chemical Engineering Science

journal homepage: www.elsevier.com/locate/ces

The flow inside shaking flasks and its implication for mycelial cultures

C. Palacios-Morales [a], J.P. Aguayo-Vallejo [b], M.A. Trujillo-Roldán [c], R. Zenit [d], G. Ascanio [b], M.S. Córdova-Aguilar [b,*]

[a] Facultad de Ingeniería, Universidad Nacional Autónoma de México, C.U., Ciudad de México 04510, Mexico
[b] Centro de Ciencias Aplicadas y Desarrollo Tecnológico, Universidad Nacional Autónoma de México, C.U., Ciudad de México 04510, Mexico
[c] Instituto de Investigaciones Biomédicas, Universidad Nacional Autónoma de México, C.U., Ciudad de México 04510, Mexico
[d] Instituto de Investigaciones en Materiales, Universidad Nacional Autónoma de México, C.U., Ciudad de México 04510, Mexico

HIGHLIGHTS

- A hydrodynamic analysis for three shaking flask geometries is presented.
- Velocity fields were experimentally measured by Particle Image Velocimetry technique.
- Strain rate is the hydrodynamic variable which strongly influences the cultures.
- This work contributes to understand more the physics of the flow inside shaken flasks.

GRAPHICAL ABSTRACT

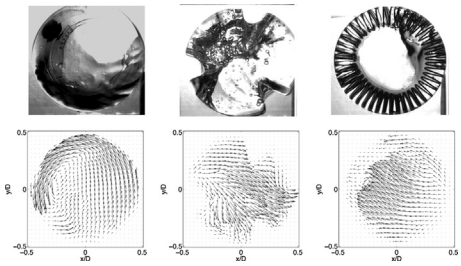

ARTICLE INFO

Article history:
Received 26 January 2016
Received in revised form
3 June 2016
Accepted 6 June 2016
Available online 7 June 2016

Keywords:
Shake flasks
PIV technique
Flow patterns
Streptomyces lividans

ABSTRACT

Several parameters such as mixing time, power consumption and deformation rates have been commonly reported in the literature for the hydrodynamic characterization of shaken flasks. In the present work, flow fields of orbital shaken flasks having different geometries have been experimentally obtained. Conventional, baffled and coiled flasks were tested at constant shaking speed of 150 rpm at which the cultures are grown. Flow fields in terms of turbulence intensity and deformation rate were both determined by means of the Particle Image Velocimetry (PIV) technique. Velocity fields are strongly dependent on the flask geometry; in particular, the main flow is confined near the wall for the conventional geometry. In general, large velocity fluctuations are found in the whole flask for the baffled and coiled geometries, while the turbulence intensity is virtually zero at the center region for the conventional flask. The measurement of the average deformation rate indicates that flow obstacles, such as indentations and coiled springs, generate regions with high hydrodynamic stresses promoting the elongation and breakup of bubbles and biomass. Results from this study have been compared with previous studies finding good agreement for the same flask configurations at similar experimental conditions.

1. Introduction

The shake flask method is the most widely used technique for bioprocess optimization and culture research, because of its simplicity, low cost and easy handling (Büchs, 2001). Flasks are available in different sizes and materials, baffled, non-baffled and with other additions such as spring coils inserted at the bottom of the flask (Hopwood et al., 1985). These designs are used for different bioprocess development projects (Suresh et al., 2009), and therefore, many studies have been conducted on flasks since this shaking process was introduced into the biotechnology field at the beginning of the previous century. Different aspects of shaken

* Corresponding author.
E-mail address: marisol.cordova@ccadet.unam.mx (M.S. Córdova-Aguilar).

http://dx.doi.org/10.1016/j.ces.2016.06.016
0009-2509/

flasks have been investigated (Freedman, 1970; Büchs et al., 2000a, b; Hansen et al., 2011; Klöckner and Büchs, 2012); however, only few studies provide complete information of the inside flow. Kurata and Mita (1996) reported a qualitative description of the shaking process in plant cell cultures using a flow visualization technique. Zhang et al. (2005) and Li et al. (2013) studied the mixing and gas-liquid mass transfer rate on baffled and unbaffled flasks using computational fluid dynamics (CFD). From a similar approach, Kim and Kizito (2009) also performed numerical simulations to study the flow in a shaken system taking into account the deforming free surface and comparing their numerical results with flow visualizations at 60 rpm finding them in good agreement. Discacciati et al. (2013) developed a numerical method to study the velocity field and the interface discontinuities to describe the flow behavior in orbitally shaken bioreactors at different agitation rates. Recently, Weheliye et al. (2013) and Rodríguez et al. (2013) provided a thorough description of the dynamics of the flow occurring inside a cylindrical shaken bioreactor using phase-resolved particle image velocimetry (PIV) as well as the mixing time data obtained with a colorimetric pH technique. Several parameters are used for the hydrodynamic characterization of stirred vessels and shaken flasks, namely: power consumption, mixing times and flow fields. Giese et al. (2014) developed an empirical correlation to determine the effective shear rate of fermentation broths in shaken flasks. For that purpose, the specific power drawn of flasks placed in an orbital shaker was measured. Although the obtained correlation is valid for a limited shake flask volume range, it could be applied for scaling up purposes. In regard to mixing times, Tan et al. (2011) used the colorimetry technique to measure the dispersing time of a tracer into the rotating bulk of a shaken flask; they observed that mixing time was similar irrespective of the shaking diameters. On the other hand, the specific power consumption in shaken flasks was measured by Peter et al. (2006) finding that more power is needed when increasing the shaking frequency and decreasing filling volume.

Nevertheless, there is still limited understanding of the flow physics and lack of engineering studies for shaken vessels, which would be required to assure reproducible and meaningful scaling-up to bioreactors (Suresh et al., 2009). In particular, the geometrical arrangement may play an important role on the quality of the mixing process in biotechnological applications. For instance, Gamboa-Suasnavart et al. (2011) reported a significant influence of the flask configuration on the production of the recombinant Ala-Pro-rich O-protein (rAPA) from *Mycobacterium tuberculosis* produced by *Streptomyces lividans*. This process has been proposed to generate part of a new tuberculosis vaccine and for diagnosis kits. They performed measurements in three shake flask configurations (conventional, baffled and with coiled spring) and evaluated the production of rAPA. Some of the differences in production were the aggregation morphology, productivity and the glycosylation properties of the recombinant protein. It was observed that the quality of the rAPA (measured as the amount of mannose residues attached to the C-terminal of the protein) increased in coiled and baffled flasks in comparison with the conventional ones. The authors firstly attributed these significant differences to the aeration/hydrodynamic stresses generated by the flask configuration. Moreover, dissimilar volumetric power inputs for the three configurations were observed for the same shaking velocity (Marín-Palacio et al., 2014). More recently, Mancilla et al. (2015) studied the flow behavior in shaken flasks using the PIV technique based on Gamboa-Suasnavart et al. (2011) flask configurations. They performed experiments at different shaking velocities ranging from 25 to 250 rpm. They found that at high shaking rates the turbulent distribution increased for all flask configurations; however, the highest turbulent production for all geometric conditions occurred at a shaking speed of about 150 rpm which is the frequency used by different authors (Gamboa-Suasnavart et al., 2011, 2013; Marín-Palacio et al., 2014). Rodríguez et al. (2015) reported a study on the effect of a conical bottom flask in an orbital shaker. They found that similar flow dynamics are obtained at lower shaking rates compared to flat bottom flasks, resulting in lower shear rates. The results reported in this paper are a continuation of Mancilla et al. (2015). In contrast to what was previously reported, we focus the investigation on a single shaking speed and only three flask geometries, searching for the dominant hydrodynamic parameters that explain the influence of the flask geometry on the production of the recombinant glycoprotein rAPA. Particular attention was paid to the flow deformation rate and turbulence intensity inside the flasks. We show that these parameters greatly influence the performance of the system in bio-culture growth. It is important to remark that the term *turbulence intensity* used in the present study, represents the turbulence of the global shaking cycle and includes the contribution from both the velocity fluctuations and the cyclic nature of the flow. In that case, this kind of turbulence is commonly known as *pseudo-turbulence*. The latter term was used throughout the text in order to be in line with common papers in chemical and biochemical engineering (Ducci and Yianneskis, 2006).

1.1. Background: culture conditions and biomass properties

In this section we discuss some results obtained by Gamboa-Suasnavart et al. (2011) and Marín-Palacio et al. (2014) which are summarized in Table 1. These authors used the wild type *Streptomyces lividans* 66 strain 1326 (Kieser et al., 2000) transformed with plasmid pIJ6021MT-45 which carries the *M. tuberculosis apa* gene under a thiostrepton-inducible promoter, conferring also resistance to kanamycin (Lara et al., 2004). Flask cultures were made in triplicates using the conventional, three baffled and coiled flask configurations of 250 ml (filled with 50 ml) Erlenmeyer flasks (Pyrex, Mexico). The flasks were shaken at 30 °C and 150 rpm during 60 h using a New Brunswick Scientific lab shaker. Analytical determinations such as biomass concentration, total protein, electrophoresis and Western blots were used for quantification, purification and identification of rAPA production as well as to obtain the morphological measurements (average diameter and roundness) which were described by Gamboa-Suasnavart et al. (2011) and Marín-Palacio et al. (2014). Also, the characterization of O-linked glycans at the C-terminal region of rAPA was made by MALDI-TOF analysis as reported by Marín-Palacio et al. (2014). The measurement of the volumetric power input (P/V) was obtained

Table 1
Morphological measurements and analytical determinations during the cultivation of *Streptomyces lividans*. Data from Gamboa-Suasnavart et al. (2011) and Marín-Palacio et al. (2014).

Shake Flask	Conventional	Baffled	Coiled
Volumetric power input (kW/m^3)	0.20	0.51	0.44
Final biomass concentration (g/L)	2.1 ± 1.2	5.6 ± 0.2	5.2 ± 0.1
Average diameter (μm)	370 ± 82 up to 700	150 ± 37	170 ± 42
Morphology of *S. lividans*	Larger pellets Rounded shape compacted	Small clumps Less compact	Smaller clumps Less compact
Final concentration of rAPA (μg/μL)	0.3	0.5	0.7
O-mannosylation pattern in the C-terminal	Up to 2 mannoses	Up to 5 mannoses	Up to 6 mannoses

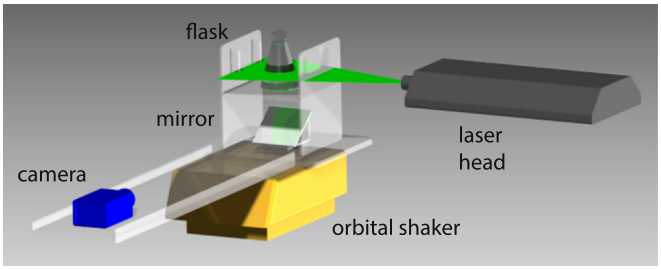

Fig. 1. Experimental setup.

using the method described by Büchs et al. (2000a,b); this method is based on torque measurements of the shaking machine with appropriate compensation of the friction losses.

From Table 1 it may be observed that the highest volumetric power input (0.51 kW/m^3) corresponded to the baffled flask configuration, which is more than twice the value of the conventional case. The presence of indentations or springs in flasks affected significantly the biomass production which was 5.6 ± 0.2 g/L for baffled and 5.2 ± 0.1 g/L for coiled configurations in contrast with the measured 2.1 ± 1.2 g/L for the conventional flask (Marín-Palacio et al., 2014). The size of pellets was measured at the end of 60 hours mixing. The largest and roundest pellets were obtained in the conventional flask with a wide range of average diameters, from 370 ± 82 up to 700 μm. For this particular case, the pellets were compact at the center of the flask and fluffy at the peripheral region. This morphology may produce diffusion limitations and affected the incorporation of the inducer thiostrepton in the mixture, reducing in consequence, the production of recombinant protein rAPA and affecting the mechanisms involved in its post-translational modifications (Córdova-Dávalos et al., 2014). On the other hand, small, dispersed mycelial aggregates and less compact clumps with oval shape were obtained in baffled and coiled shake flask cultures. The average diameter for both configurations was approximately 160 ± 40 μm, with a narrow distribution and approximately 60% smaller than the average diameter of conventional flasks (Marín-Palacio et al., 2014). Additionally, the SDS-PAGE method and densitometry demonstrated almost 3 times higher production of rAPA in coiled and baffled flasks than in the conventional ones (Gamboa-Suasnavart et al., 2011). The recombinant protein (rAPA) was purified and digested with LysC, producing at least eight peptides and the C-terminal peptide had the major variability in *O*-mannosylation (Gamboa-Suasnavart et al., 2011). The small and dispersed mycelial aggregates obtained in baffled and coiled flasks improve the degree of *O*-mannosylation of the recombinant protein up to 6 mannose residues attached to the carboxy-terminal region in comparison with the large pellets obtained in conventional flasks which produced only two mannose residues.

2. Materials and methods

2.1. Experimental setup

Three different configurations of 250 ml Erlenmeyer flasks (Pyrex, Mexico) were tested: conventional, baffled and coiled; as mentioned before, we used the same flask configurations as Gamboa-Suasnavart et al. (2011), Marín-Palacio et al. (2014) and Mancilla et al. (2015). The conventional flask had a standard design which consists of a round circular shape at the bottom section. Baffled flask had three 45° indentations placed at 120° with 20 mm depth and 45 mm height as described in detail elsewhere (Zirkle et al., 2004; Gamboa-Suasnavart et al., 2011). Coiled flask consisted of a conventional flask with a 30 cm stainless steel spring (1.3 cm diameter, 19 SW) inserted inside, as previously described (Hopwood et al., 1985; Zirkle et al., 2004; Gamboa-Suasnavart et al., 2011). In order to have similar fluid characteristics, each flask was filled with 50 ml of Luria-Bertani's medium modified by the addition of 34 w/v sucrose (Gamboa-Suasnavart et al., 2011; Marín-Palacio et al., 2014; Mancilla et al., 2015), with the following properties: density $\rho = 1300$ kg/m^3, viscosity $\eta = 3.5$ mPa·s and surface tension $\sigma = 62$ N/m. These properties were measured at 23 °C with a density scale, a 50 mm diameter cone-plate in a controlled stress rheometer (MCR101 Anton Paar) and a Wilhelmy plate respectively. The flasks were agitated in an orbital standard shaker (VWR, model Signature DS-500), with a counter-balanced eccentric drive mechanism that travels over a 19 mm (3/4 in) circular orbit (shaking diameter) at speed rate of 150 rpm (shaking frequency) for all tests. At this speed, the fluid covered the entire base of the flasks. A schematic diagram of the experimental setup is shown in Fig. 1. The flask was mounted onto a transparent support made of plexi-glass; a mirror with an inclination of 45° was placed below to observe the flask from the bottom. In order to minimize optical distortion, the flask was placed inside a square jacket and the space between the walls of the flask and the jacket was filled with glycerol. A CCD camera was mounted on a horizontal arm which moved with the whole flask support.

2.2. Velocity measurements

The 2D velocity fields were obtained using a Dantec Dynamics particle image velocimetry (PIV) system. A Nd:YAG laser (New Wave Solo III 50 mJ) was used to generate a laser sheet of 532 nm (green light). The CCD camera (Kodak Megaplus, Model ES 1.0) with a 35 mm lens (F1.65 Edmund Optics) was placed in front of the mirror and the horizontal laser sheet was aligned parallel to the flask bottom with a height of 3 mm from the bottom. The incorporation of air bubbles during the shaking caused some laser reflections; for this reason, fluorescent polyamide particles with an average diameter of 10 μm were used as particle tracers and an optical filter (550 nm) was placed in front of the camera lens. A cross-correlation algorithm was used to obtain the velocity fields (in Cartesian coordinate system) using an interrogation area of 32×32 pixels and an overlap of 50% obtaining a spatial resolution of 1.53 mm^2. Standard PIV validation and filtering techniques were used (peak validation, moving average validation, average filter, etc.) to eliminate spurious vectors. We determined that for the largest agitation (the baffled flask) the amount of spurious vectors was at most 10% of the total. The experimental sampling rate (frequency) was 4 Hz; however, for some tests, the phase locking technique was used to perform the acquisitions at the same position of the shaking cycle. For this purpose, an optical detector coupled to an electronic device generated a TTL signal every time it was interrupted by the shaking motion. This signal was used to synchronize both the image acquisition and the flow phase in the flask; at least, 300 images were taken in all cases to obtain statistically averaged data. The flow behavior at the bottom view of

the flask was studied by means of a high speed video camera (MotionPro HS-4, Redlake, USA). For these tests, the illumination was provided by a high intensity LEDs lamp that was placed at the top of the experimental setup; a light diffuser was placed in front of the lamp to increase the contrast at the interface. Image sequences were acquired at 300 frames per second in all cases.

The shaking velocity is defined as $U_{sh} = 2\pi fR$; where f is the shaking velocity in [rev/s] and R is the flask radius. Since the main flow inside the flasks is circular, the original two-dimensional Cartesian coordinates (x, y) are converted into a polar coordinate (r, θ) system. In turn, the Cartesian velocity vectors (u_x, u_y) are transformed into the polar coordinates (u_r, u_θ); where u_r and u_θ are the radial and tangential velocities respectively, with the flask center at (0, 0). The velocity magnitude, for every point, is defined as

$$U = \left(u_r^2 + u_\theta^2\right)^{1/2}. \tag{1}$$

The degree of mixing is well known to depend on the intensity of the flow fluctuations (Pope, 2000). Therefore, we obtained a measurement of the fluctuations by considering the standard deviation of the velocity components (u_r', u_θ') as a function of time. The pseudo-turbulence intensities for the radial and tangential

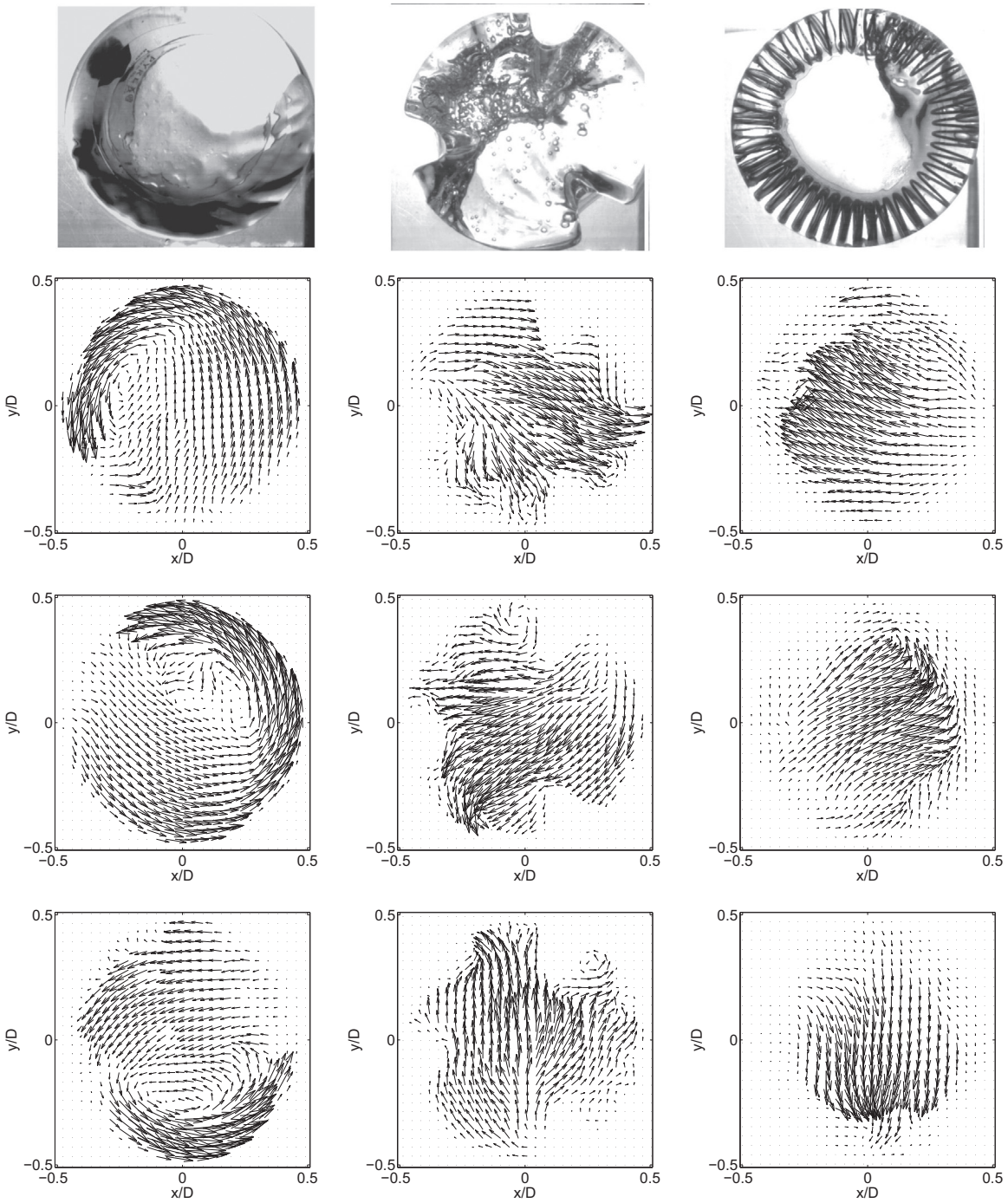

Fig. 2. Flow behavior. First row: still images of conventional (left), baffled(center) and coiled (right) shaken flasks. Rows 2, 3 and 4: instantaneous velocity fields with $\Delta t = 250$ ms.

components were calculated for each position considering:

$$I_r = \frac{u_r'}{U_{sh}} \tag{2}$$

$$I_\theta = \frac{u_\theta'}{U_{sh}}. \tag{3}$$

In addition to the pseudo-turbulence intensity, some studies have shown that the strength of the deformation rate (both shear and extension rates) can affect the integrity of cell cultures (Kroll et al., 1996; Trujillo-Roldán and Valdez-Cruz, 2006) and even proteins (Schneider et al., 2007). Since we have detailed information about the velocity fields, the rate of deformation tensor of the flow can be calculated as

$$\boldsymbol{D} = \frac{1}{2}((\nabla \boldsymbol{u}) + (\nabla \boldsymbol{u})^t) \tag{4}$$

where $\nabla \boldsymbol{u}$ is the velocity gradient tensor. The magnitude of the

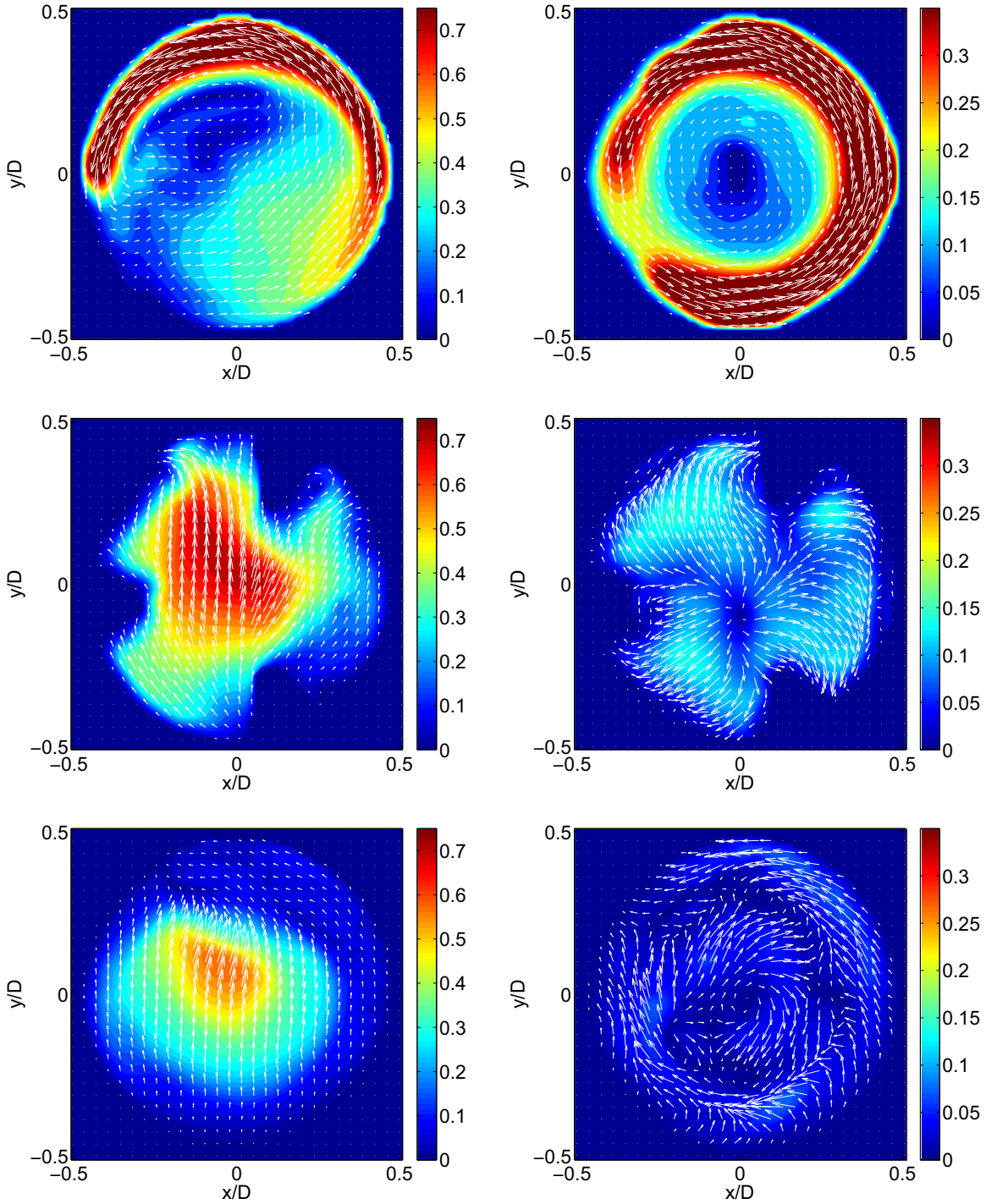

Fig. 3. Averaged velocity magnitude U/U_{sh} for: conventional, baffled and coiled configurations (from top to bottom row). Left column: phase locked. Right column: time average.

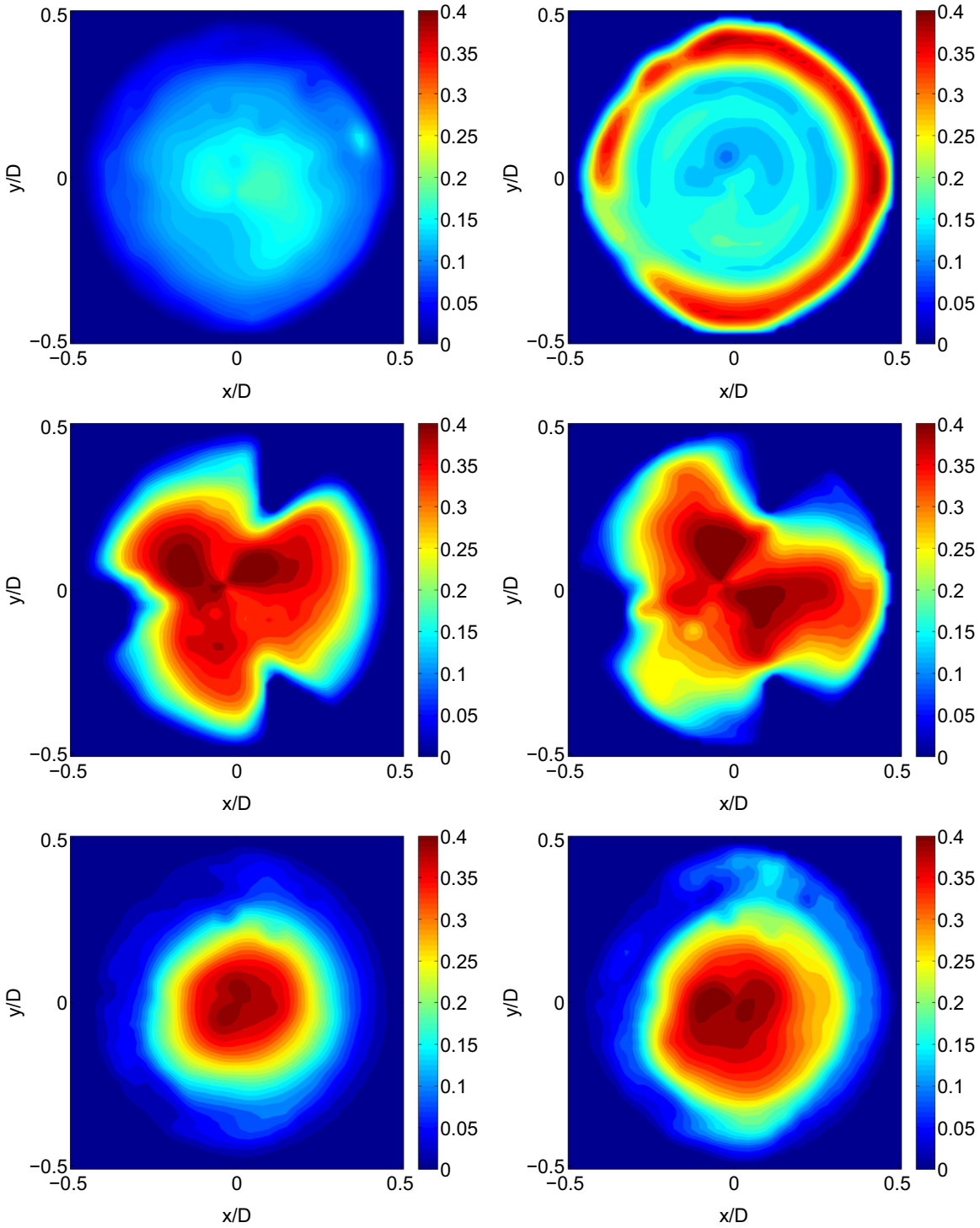

Fig. 4. Radial (left) and tangential (right) pseudo-turbulence intensities for: conventional, baffled and coiled configurations (from top to bottom row).

rate of deformation can be obtained point-by-point in the domain by computing $|\boldsymbol{D}| = \mathrm{tr}[\boldsymbol{D}\boldsymbol{D}^t]^{1/2}$. Note that this way to calculate the size of $\boldsymbol{D}$ accounts for both shear and extension rates of the flow.

3. Results and discussion

The first row of Fig. 2 shows still images from the bottom view of all flasks at 150 rpm; from left to right: conventional, baffled and coiled configurations. The deformation of the interface can be identified by dark regions in the images. Clearly, the fluid motion is different for the three flaks configurations; in general, the flow behavior depends on the flask geometry and the shaking speed (Mancilla et al., 2015). For the conventional flask, the liquid tends to accumulate at one edge of the flask wall increasing the liquid depth and velocity in this region. This fluid 'crest' moves in the tangential direction as the flask is shaken forming a solid-like movement which can be in-phase (or not) with the flask motion depending on the flow and geometric characteristics (Büchs et al., 2000a). For this case, waves at the interface are observed. For the baffled configuration, we observe that the liquid interacts strongly with the flask indentations generating an asymmetrical flow; the

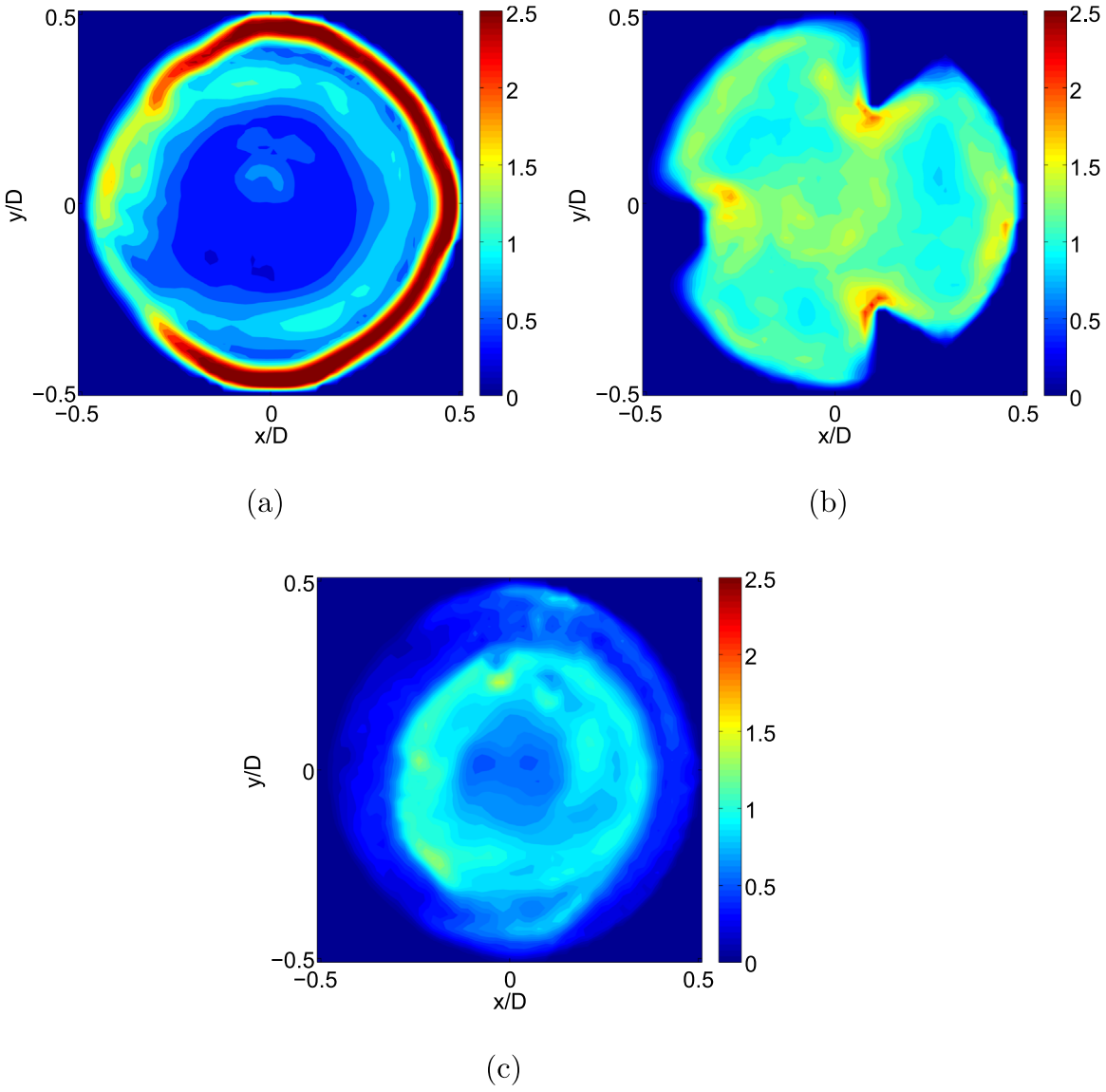

Fig. 5. Averaged deformation rate magnitude $|\boldsymbol{D}|/(U_{sh}/R)$ for (a) conventional, (b) baffled and (c) coiled flask configurations.

formation of important secondary fluid streams in the radial direction is also observed. The incorporation of air into the liquid bulk is also noticeable, which leads to the formation, break up and coalescence of bubbles. For the coiled configuration we observe that the liquid interacts with the steel spring promoting the formation of smaller bubbles with uniform size which remain mostly trapped inside the coil. A stronger and faster flow is observed at the central region of the flask. On the other hand, for the conventional flask, the interface was not sufficiently deformed to allow the incorporation of air. Rows 2, 3 and 4 from Fig. 2 show typical instantaneous velocity fields for the three flask configurations, at different time instants with $\Delta t = 250$ ms. The axis x and y are scaled with the flask diameter and the origin is located at the center of the flask. For the conventional flask case, we observe that the main flow is located at the periphery of the flask; it is possible to observe the motion of the fluid interface represented as the increment of the fluid velocity near the flask wall. In comparison, the velocity at the center of the flask is smaller. A more complex flow behavior is observed for the baffled configuration because the main flow is disrupted by the indentations, producing circulation in many directions and vortices at the corners of these indentations. Meanwhile, a stronger flow is observed at the center of the flask. On the other hand, for the coiled flask, we observe that the fluid interacts with the steel spring in such a way that two flow regions are generated; one inside the coil and another at the center of the flask.

In Fig. 3 we show the normalized velocity magnitude, U/U_{sh}, for the three flask configurations. The velocity magnitude, displayed in color scale, is averaged over time (75 s); the white arrows represent the averaged velocity fields. On the left column we show the velocity magnitude for a specific flask position obtained with the phase locking technique; on the other hand, on the right column we show the time-averaged velocity magnitude, obtained with a sampling frequency of 4 Hz. Clearly, these two averaging strategies provide slightly different description of the flow. Evidently, when using phase locking (left column), the velocities for a specific instant of the shaking cycle are observed (Weheliye et al., 2013; Rodríguez et al., 2013). The time average, in turn, gives a global description of the fluid motion through the entire cycle. In consequence, the velocity magnitude changes when different phases of the flow are considered as observed on the right column of Fig. 3. For the conventional configuration we observe that the main flow remains on the flask periphery, while the flow at the flask center is virtually non-existent. On the contrary, for the

baffled flask, the velocity magnitude indicates that the main flow starts at the center of the flask and is directed radially toward the flask walls. A more complex and three dimensional flow behavior is observed for the coiled configuration, however, some features are still discernibles: a relatively fast counterclockwise flow inside the steel spring and a slower flow at the flask center. From the phase locked velocity data (left column of Fig. 3), we were able to obtain statistical information of the flow for a specific instant of the shaking cycle because the flow is essentially in-phase with the flask motion. In consequence, it is not possible to obtain the flow fluctuations of the overall shaking cycle unless different instants of the cycle are considered. In contrast, the statistical information of the time-averaged velocity data allows to study the velocity fluctuations for different phases of the shaking cycle, giving a more global description of the process. Such differences in the analysis of these two ways to obtain statistical measurements can be observed in Fig. 3 (right and left columns for all flask configurations). Therefore, we present results only for the experiments with a sampling frequency of 4 Hz (right column of Fig. 3), which correspond to the case of the time-averaged scheme.

In Fig. 4 we show the pseudo-turbulence intensities for all flask configurations. On the left and right columns, we show the radial I_r and tangential I_θ pseudo-turbulence intensities, respectively. For the conventional flask (first row) we observe that the tangential pseudo-turbulence intensity is dominant. In other words, the velocity fluctuations in the radial direction are very low for this configuration. This is not the ideal condition because the mixing (and therefore, the mass transfer) along the radial layers of the flow is relatively poor. In contrast, for the baffled configuration we observe that the radial and tangential pseudo-turbulence intensities are comparable in value. In particular, we observe that there is good mixing in the radial direction (left column) in all regions of the flask. The maximum pseudo-turbulence intensities are located close to the center of the flask. For the coiled configuration we also observe that both pseudo-turbulence intensities are similar in the flask domain. The maximum pseudo-turbulence intensities are also located at the center of the flask. However, the pseudo-turbulence intensity inside the metallic spring is relatively low. It is possible that the coil dampens the fluid motion making the flow at the flask periphery more homogeneous and reducing flow fluctuations. As stated before, the pseudo-turbulence intensities shown in Fig. 4 represent the turbulence of the global cycle and include the contributions from both the velocity fluctuations and the cyclic nature of the flow, which in turn influence the biomass production. To properly study and separate the turbulence contributions one would have to obtain measurements with the phase-locked scheme in different instants of the cycle (Escudié and Liné, 2003; Ducci and Yianneskis, 2006). We plan to pursue such an investigation in the future.

The magnitude of the deformation rate in the flow is shown in Fig. 5. The strain-tensor (Eq. (4)) is computed for each instantaneous velocity field and then averaged in time; the strain-rate values are normalized by $|\boldsymbol{D}|/(U_{sh}/R)$. In flow regions with large $|\boldsymbol{D}|$, the fluid is subjected to high hydrodynamic stresses promoting the rupture of large bubbles or particles. The time averaged deformation allows to locate the regions of flow with the highest stress during the entire shaking cycle. For the conventional configuration (Fig. 5a), there is a very thin region where the strain rate is large; this region is located along the periphery of the flask, while in the rest of the flask area, the strain values are comparatively small. This means that the hydrodynamic stresses are concentrated only close to the flask wall for this configuration. These regions coincide with those obtained for the pseudo-turbulence intensities results as shown in Fig. 4. For the baffled flask, (Fig. 5b), we clearly observe that there are different regions with high stress; particularly, close to the tip of the baffles the strain-rate is relatively large. Therefore, in these regions of flow, there are large velocity gradients which may produce solid particles and bubbles to deform, elongate and eventually break into smaller ones. In general, we observe that the hydrodynamic stress in the baffled flask is more homogeneous compared to the conventional configuration. Finally, for the coiled flask configuration, (Fig. 5c), we observe that the largest strain-rate values are located in the region where bulk central flow interacts with the string. Therefore in this region, particles are subjected to large stress and they are susceptible to break. The distribution of the strain-rate is roughly axisymmetric for this case.

4. Conclusions

Flow fields of orbital shaken flasks have been experimentally obtained by means of the Particle Image Velocimetry technique. The effect of the flask geometry has been analyzed at constant shaking rate in terms of pseudo-turbulence intensity and deformation rate. For that purpose, three different flask geometries have been investigated, namely: conventional, baffled and coiled. In the case of the conventional geometry, velocity fields reveal the confinement of the main flow near the wall resulting in nearly zero turbulence intensity at the center. On the other hand, large velocity fluctuations were observed in the whole flask for the coiled and baffled geometries. In those geometries, the measurement of the average deformation rate indicate that the obstacles generate regions with high hydrodynamic stress, which favor the elongation and breakup of bubbles and biomass. From the culture results, it may be inferred that the performances of the baffled and coiled configurations are similar, though the latter is slightly better. In contrast, experiments in the conventional flask resulted in lower concentrations of biomass, rAPA, and number of mannoses attached to the C-terminus of the protein. Average pellet diameter and *S. lividans* morphology were also influenced by the flask setup: larger pellets (presenting mass diffusion problems) are obtained for the conventional case while smaller and less compact ones for the other two types of flasks. Based on all these observations, uniform distributions of deformation-rate values and pseudo-turbulence intensities are desirable, in order to improve mixing (along with oxygen uptake) and for the *S. lividans* case, an improvement on culture quality.

References

Büchs, J., 2001. Introduction to advantages and problems of shaken cultures. Biochem. Eng. J. 7, 91–98.
Büchs, J., Maier, U., Milbradt, C., Zoels, B., 2000a. Power consumption in shaking flasks on rotary shaking machines: I. Power consumption measurement in unbaffled flasks at low liquid viscosity. Biotechnol. Bioeng. 68, 589–593.
Büchs, J., Maier, U., Milbradt, C., Zoels, B., 2000b. Power consumption in shaking flasks on rotary shaking machines: II. Nondimensional description of specific power consumption and flow regimes in unbaffled flasks at elevated liquid viscosity. Biotechnol. Bioeng. 68, 594–601.
Córdova-Dávalos, L.E., Espitia, C., González-Cerón, G., Arreguín-Espinosa, R., Soberón-Chávez, G., Servín-González, L., 2014. Lipoprotein N-acyl transferase (Lnt1) is dispensable for protein O-mannosylation by *Streptomyces coelicolor*. FEMS Microbiol. Lett. 350, 72–82.
Discacciati, M., Hacker, D., Quarteroni, A., Quinodoz, S., Tissot, S., Wurm, F.M., 2013. Numerical simulation of orbitally shaken viscous fluids with free surface. Int. J. Numer. Meth. Fluids 71, 294–315.
Ducci, A., Yianneskis, M., 2006. Turbulence kinetic energy transport processes in the impeller stream of stirred vessels. Chem. Eng. Sci. 61, 2780–2790.
Escudié, R., Liné, A., 2003. Experimental analysis of hydrodynamics in a radially agitated tank. AIChE J. 49, 585–603.
Freedman, D., 1970. The shaker in bioengineering. Method Microbiol. 2, 175–185.
Gamboa-Suasnavart, R.A., Marín-Palacio, L.D., Martínez-Sotelo, J.A., Espitia, C., Servín-González, L., Valdez-Cruz, N.A., Trujillo-Roldán, M.A., 2013. Scale-up from shake flasks to bioreactor based on power input and *Streptomyces lividans* morphology for the production of recombinant APA (45/47 kDa protein) from

Mycobacterium tuberculosis. World J. Microbiol. Biotechnol. 29, 1421–1429.
Gamboa-Suasnavart, R.A., Valdéz-Cruz, N.A., Córdova-Dávalos, L.E., Martínez-Sotelo, J.A., Servín-González, L., Espitia, C., Trujillo-Roldán, M.A., 2011. The O-mannosylation and production of recombinant APA (45/47 kDa) protein from *Mycobacterium tuberculosis* in *Streptomyces lividans* is affected by culture conditions in shake flasks. Microb. Cell. Fact. 10, 110–120.
Giese, H., Klöckner, W., Peña, C., Galindo, E., Lotter, S., Wetzel, K., Meissner, L., Peter, C.P., Büchs, J., 2014. Effective shear rates in shake flasks. Chem. Eng. Sci. 118, 102–113.
Hansen, S., Kensy, F., Käser, A., Büchs, J., 2011. Potential errors in conventional dot measurement techniques in shake flasks and verification using a rotating flexitube optical sensor. BMC Biotechnol. 11, 49.
Hopwood, D.A., Bibb, M., Kieser, T., Bruton, C., Kieser, H., Lydiate, D., Smith, C., Ward, J., Schrempf, H., 1985. Genetic Manipulation of Streptomyces: A Laboratory Manual. The John Innes Foundation, UK.
Kieser, T., Bibb, M., Buttner, M., Chater, K., Hopwood, D., 2000. Practical Streptomyces Genetics. John Innes Foundation, UK.
Kim, H.M., Kizito, J.P., 2009. Stirring free surface flows due to horizontal circulatory oscillation of a partially filled container. Chem. Eng. Commun. 196, 1300–1321.
Klöckner, W., Büchs, J., 2012. Advances in shaking technologies. Trends Biotechnol. 30, 307–314.
Kroll, M.H., Hellums, J.D., McIntire, L., Schafer, A., Moake, J., 1996. Platelets and shear stress. Blood 88, 1525–1541.
Kurata, K., Mita, H., 1996. Qualitative analysis of liquid movement within shake culture flasks using a flow visualization technique. Acta Hortic. 440, 545–548.
Lara, M., Servín-González, L., Singh, M., Moreno, C., Cohen, I., Nimtz, M., Espitia, C., 2004. Expression, secretion, and glycosylation of the 45- and 47-kDa glycoprotein of *Mycobacterium tuberculosis* in *Streptomyces lividans*. Appl. Environ. Microb. 70, 679–685.
Li, C., Xia, J.-Y., Chu, J., Wang, Y.-H., Zhuang, Y.-P., Zhang, S.-L., 2013. CFD analysis of the turbulent flow in baffled shake flasks. Biochem. Eng. J. 70, 140–150.
Mancilla, E., Palacios-Morales, C., Córdova-Aguilar, M., Trujillo-Roldán, M., Ascanio, G., Zenit, R., 2015. A hydrodynamic description of the flow behavior in shaken flasks. Biochem. Eng. J. 99, 61–66.
Marín-Palacio, L.D., Gamboa-Suasnavart, R.A., Valdez-Cruz, N.A., Servín-González, L., Córdova-Aguilar, M.S., Soto, E., Klöckner, W., Büchs, J., Trujillo-Roldán, M.A., 2014. The role of volumetric power input in the growth, morphology, and production of a recombinant glycoprotein by Streptomyces lividans in shake flasks. Biochem. Eng. J. 90, 224–233.
Peter, C.P., Suzuki, Y., Rachinskiy, K., Lotter, S., Büchs, J., 2006. Volumetric power consumption in baffled shake flasks. Chem. Eng. Sci. 61, 3771–3779.
Pope, S.B., 2000. Turbulent Flows. Cambridge University Press, New York.
Rodríguez, G., Pieralisi, I., Anderlei, T., Ducci, A., Micheletti, M., 2015. Appraisal of fluid flow in a shaken bioreactor with conical bottom at different operating conditions. Chem. Eng. Res. Des. . http://dx.doi.org/10.1016/j.cherd.2015.12.012
Rodríguez, G., Weheliye, W., Anderlei, T., Micheletti, M., Yianneskis, M., Ducci, A., 2013. Mixing time and kinetic energy measurements in a shaken cylindrical bioreactor. Chem. Eng. Res. Des. 91, 2084–2097.
Schneider, S., Nuschele, S., Wixforth, A., Gorzelanny, C., Alexander-Katz, A., Netz, R., Schneider, M., 2007. Shear-induced unfolding triggers adhesion of von Willebrand factor fibers. Proc. Natl. Acad. Sci. USA 104, 7899–7903.
Suresh, S., Srivastava, V., Mishra, I., 2009. Critical analysis of engineering aspects of shaken flask bioreactors. Crit. Rev. Biotechnol. 29, 255–278.
Tan, R.-K., Eberhard, W., Büchs, J., 2011. Measurement and characterization of mixing time in shake flasks. Chem. Eng. Sci. 66, 440–447.
Trujillo-Roldán, M.A., Valdez-Cruz, N.A., 2006. El estrés hidrodinámico muerte y daño celular en cultivos agitados. Rev. Latinoam. Microbiol. 48, 269–280.
Weheliye, W., Yianneskis, M., Ducci, A., 2013. On the fluid dynamics of shaken bioreactors flow characterization and transition. AIChE J. 59, 334–344.
Zhang, H., Williams-Dalson, W., Keshavarz-Moore, E., Shamlou, P.A., 2005. Computational-fluid-dynamics (CFD) analysis of mixing and gas–liquid mass transfer in shake flasks. Biotechnol. Appl. Bioc. 41, 1–8.
Zirkle, R., Ligon, J.M., Molnár, I., 2004. Heterologous production of the antifungal polyketide antibiotic soraphen A of *Sorangium cellulosum* So ce26 in *Streptomyces lividans*. Microbiology 150, 2761–2774.